SCIENTIFIC REPORTS

OPEN

SUBJECT AREAS:
ELECTRONIC DEVICES
SOLAR CELLS

Received
24 April 2014

Accepted
21 July 2014

Published
10 October 2014

Correspondence and requests for materials should be addressed to J.H.H. (hjhzlz@iccas.ac.cn); B.F. (fanbin@weihua-solar.com) or M.L.S. (mlsun@ouc.edu.cn)

* These authors contributed equally to this work.

Ultrathin Polyaniline-based Buffer Layer for Highly Efficient Polymer Solar Cells with Wide Applicability

Wenchao Zhao[1,2]*, Long Ye[1]*, Shaoqing Zhang[1], Bin Fan[3], Mingliang Sun[2] & Jianhui Hou[1]

[1]State Key Laboratory of Polymer Physics and Chemistry, Beijing National Laboratory for Molecular Sciences Institute of Chemistry, Chinese Academy of Sciences, Beijing 100190, P. R. China, [2]Institute of Material Science and Engineering, Ocean University of China, Qingdao 266100, P. R. China, [3]Xiamen Weihua-solar Co. Ltd, Xiamen 361115, P. R. China.

Interfacial buffer layers often attribute the improved device performance in organic optoelectronic device. Herein, a water-soluble hydrochloric acid doped polyanilines (HAPAN) were utilized as *p*-type electrode buffer layer in highly efficient polymer solar cells (PSC) based on PBDTTT-EFT and several representative polymers. The PBDTTT-EFT-based conventional PSC featuring ultrathin HAPAN (1.3 nm) delivered high *PCE* approximately 9%, which is one of the highest values among conventional PSC devices. Moreover, ultrathin HAPAN also exhibited wide applicability in a variety of efficient photovoltaic polymers including PBDTTT-C-T, PTB7, PBDTBDD, PBTTDPP-T, PDPP3T and P3HT. The excellent performances were originated from the high transparency, small film roughness and suitable work function.

During the past decades, electrode buffer layers have played a vital role in promoting the performance of organic optoelectronic devices, in particular for organic photovoltaic devices (as shown in Figure 1a), which consist of electrodes (anode and cathode), photoactive layers, and electrode buffer layers (EBLs)[1–4]. Both inorganic and organic materials can be used for making the EBLs. Recently, important progresses have been achieved in developing new *n*-type organic EBLs, and the power conversion efficiencies (*PCEs*) of polymer solar cells (PSCs) over 8% have been achieved in various groups via polymer interlayers such as amino-substituted polyfluorene derivatives (PFN)[5–9], ethoxylated polyethyleneimine (PEIE)[10], fullerene derivatives[11,12]. Compared to the rapid progresses in *n*-type organic EBL materials, the development of solution processable *p*-type organic materials is comparatively lagged behind. Although, the applications of a few *p*-type organic materials in PSCs were reported in recent works[13–16], the classical *p*-type EBL material, poly(3,4-ethylenedioxythiophene):poly(styrenesulfonate) (PEDOT: PSS), is predominantly used as the *p*-type EBL material in PSCs, and also the highest *PCE* values in PSCs were obtained by utilizing PEDOT: PSS as EBLs[17]. To explore a new solution processable organic *p*-type EBL material with superior properties is still an interesting and important topic for the field of PSCs.

A superior *p*-type organic EBL material should meet several requirements: (i) Processing solvent of the buffer layer should be orthogonal with that of the active layer. (ii) As known, the state-of-the-art donor polymers often exhibited HOMO levels of 5.0 ~ 5.4 eV (see Figure 1b)[18–27], and thereby the work function (WF) of the *p*-type EBL material should exceed 5.0 eV to form ohmic contact with the active layers. (iii) In PSCs, the EBL should have very high transparency and thus the active layer can utilize more sunlight. Usually, more than 5% of the incident light was loss in the 35 nm PEDOT:PSS layer. To minimize the light loss, two strategies can be considered: the first choice is to explore new materials with no or extremely low absorption in visible region; an alternative strategy is to utilize ultrathin buffer layers. For example, Heeger *et al.*[16] reported a novel *p*-type conjugated polyelectrolyte, which can fulfill all these above requirements simultaneously and thus exhibited comparable performance with PEDOT:PSS in PSCs.

As a type of classical conducting polymers, polyanilines have been widely studied in the past decades due to their high conductivities, environmental stabilities and ease of synthesis for multiple energy-related applications such as sensors, supercapacitors and organic light-emitting diodes[28–31]. Polyanilines with good solution processibilities in commonly used solvents can be prepared through internal or external doping. For instance, when doped by sulfonic acid, polyanilines can be dissolved into water[32], and the water soluble polyanilines can be used as the *p*-type EBL materials in organic solar cells[33]. A few of acid doped polyanilines like acid-doped polyaniline nanotubes (a-PANIN), self-doped sulfonic acid polyaniline (SPAN) and graft copolymers (PAN-PEG) have been

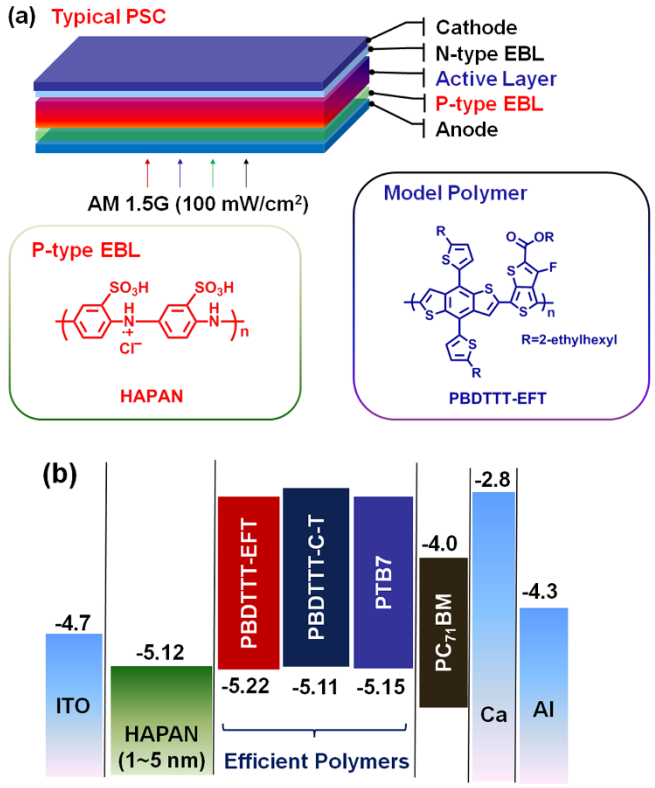

Figure 1 | (a) Device diagram of PSCs and the chemical structure of the materials involved in the current work: hydrochloric acid doped polyaniline (HAPAN) as well as the model polymer (PBDTTT-EFT); (b) Energy level diagram of the state-of-the-art photovoltaic materials.

explored in P3HT:PCBM based PSCs and achieved relatively poor or comparable performance with PEDOT: PSS[34–36]. Overall, although polyaniline based *p*-type EBLs have been utilized in classical PSCs, their applications and underlying potentials in highly efficient PSCs based on novel photovoltaic polymers have not been intensively investigated yet.

Herein, a water-soluble hydrochloric acid doped polyanilines (named as HAPAN in Figure 1a) were employed as the *p*-type EBL material in highly efficient PSCs based on Poly(2-ethylhexyl 6-(4, 8-bis(5-(2-ethylhexyl)thiophen-2-yl)benzo[1,2-b:4,5-b′]dithiophen-2-yl)-3-fluorothieno[3,4-b]thiophene-2-carboxylate) (designated as PBDTTT-EFT in Figure 1a)[11]. Notably, when the blend of PBDTTT-EFT:$PC_{71}BM$ was used as the active layer, the PSC with only 5.0 nm HAPAN film as the *p*-type EBL exhibited excellent photovoltaic performance with *PCE* exceeding 9%. Interestingly, the HAPAN-based PSC still achieved a high *PCE* up to 8.94% when the thickness of HAPAN film is reduced to only 1.3 nm under the illumination of AM 1.5G 100 mW/cm^2.

Results

HAPAN is prepared by a cost-effective method, namely a direct sulfonation of emeraldine salts with chlorosulfonic acid in dichloroethane at 80°C and subsequently hydrated in water at 100°C, and the synthesis details have been reported elsewhere[37]. The FT-IR spectrum and XPS spectra of HAPAN are provided (see Figure S1 and Table S1 in supporting information). HAPAN exhibits good solubility (up to 30 mg/ml) in water while insoluble in *o*-DCB. Under the concentration of 1 mg/ml, the corresponding pH of HAPAN solution is 4.2, which is slightly higher than that of the well-known PEDOT:PSS (VP AI 4083 from H. C. Stark, PEDOT4083).

Initially, the work functions (WF) of HAPAN films were characterized by ultraviolet photoelectron spectroscopy (UPS). Figure 2a presented the UPS results of the pristine ITO and HAPAN films with different thickness (1.3 nm, 5.0 nm and 30 nm) covered indium-tin-oxide (ITO) samples. The thicknesses of HAPAN were measured and controlled by spectroscopic ellipsometer and surface profilometer (see Figure S2a), meanwhile, the photographs of HAPAN films with different thickness were depicted in Figure S2b. The WF value of ITO measured by UPS was consistent with the reported results[35]. The WF of 30 nm HAPAN film was determined to be 5.12 eV, which is similar as the WF (5.16 eV) of PEDOT:PSS[35]. It is interesting to note that the ultrathin HAPAN film (5.0 nm) exhibited the same WF value of 5.12 eV as that of the thicker HAPAN film (30 nm). The results demonstrated that the WF of ITO can be well modified by coating 5.0 nm HAPAN buffer layer. As the thickness of HAPAN film reduced to 1.3 nm, the WF was 4.75 eV and close to that of the bare ITO film (4.72 eV).

The transmittance of the EBL is an important parameter that affects the photovoltaic performance especially short-circuit current density (J_{sc}) of PSCs. As known, the optimized thickness of the PEDOT:PSS layers are ca. 35 nm, which blocks some of solar light[38]. Figure 2b depicted the optical transmittance spectra of the HAPAN films with varied thicknesses on quartz glass in the UV-Vis-NIR region. We found that the transmittance of the 30 nm HAPAN film is lower than that of the PEDOT:PSS (35 nm)[35]. When the thickness of HAPAN reduced to 5.0 nm or even to 1.3 nm, the corresponding transmittance of the whole absorption range was 95% ~ 98%, which was much higher than that of the PEDOT:PSS film (35 nm).

Surface morphologies of the HAPAN film on the ITO coated glass were probed by tapping-mode atomic force microscopy (AFM) measurements. Height topography images and the corresponding root-mean-square roughness (R_q) were taken for each film and shown in Figure 2c. After modified with 5.0 nm HAPAN film, the R_q value of ITO is significantly reduced from 3.50 nm to 1.32 nm. Interestingly, when 1.3 nm thick HAPAN was coated, the surface roughness of ITO still can be reduced effectively, i.e. the R_q value is 1.67 nm. Clearly, the ultrathin HAPAN (1.3 nm–5.0 nm) films are suitable *p*-type buffer material to meet the three key characteristics: high transmittance, suitable WF as well as relatively smooth surface.

Recently, Benzo[1,2-*b*:4,5-*b*′]dithiophene-based photovoltaic materials like PBDTTT-EFT, PBDTTT-C-T, PTB7 made a series of outstanding progress in polymer photovoltaic field[5–8,11,19–25,38–40]. Herein, a newly developed polymer PBDTTT-EFT[11,39] was selected as the model polymer to verify the suitability of ultrathin HAPAN in highly efficient PSCs. Initially, to investigate the thickness dependence of HAPAN on photovoltaic performance, the PSCs based on PBDTTT-EFT: $PC_{71}BM$ with the conventional device configuration (ITO/*p*-type EBL/active layer/Ca/Al) were fabricated and characterized under AM 1.5G illumination (100 mW/cm^2), as depicted in Figure 3a. The optimal D/A ratio (1 : 1.5) and processing solvent (DCB/3% DIO) were consistent with the reported work[11]. As shown in Figure S3 and Table 1, when the thickness of the HAPAN buffer layer increased from 1.3 nm to 30 nm, the V_{oc} values of the devices were ca. 0.79 V, indicating that the thickness of the HAPAN film does not affect the V_{oc} of the PSC at all. Noting that the ITO anode modified with 1.3 nm HAPAN showed a WF of 4.75 eV, it is interesting to get a V_{oc} of 0.79 V for the device with 1.3 nm HAPAN. We speculate that the UPS result of the 1.3 nm HAPAN sample might be affected by the bared ITO part on the substrates, because the R_q of ITO (R_q = 3.5 nm, see Figure 2c) is much higher than the thickness of the ultrathin HAPAN (1.3 nm).

When the thickness of the HAPAN buffer layer was changed from 1.3 nm to 30 nm, the J_{sc} values kept ~15 mA/cm^2 with a peak value of 16.54 mA/cm^2 (see Figure 3b and Table 1). For the PSCs without *p*-type EBL, poor *PCE* of 4.28 ± 0.28% were recorded. When modified with 5.0 nm HAPAN, the PSCs delivered the best *PCE* (9.00 ± 0.12%) along with the highest J_{sc} of 16.51 mA/cm^2, a V_{oc} of 0.789 V, and a *FF* of 0.695, which were among the highest values from con-

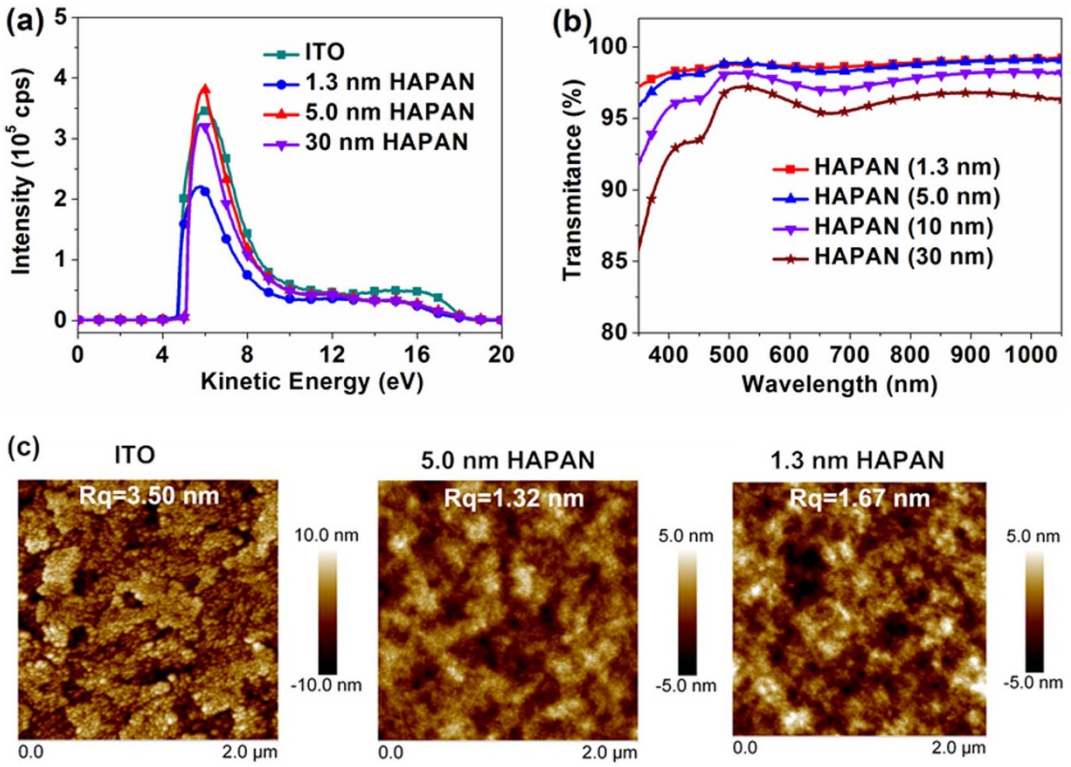

Figure 2 | (a) UPS spectra of indium-tin oxide (ITO), PEDOT: PSS (35 nm), different thickness of HAPAN (1.3 nm, 5.0 nm and 30 nm) film on ITO substrate, respectively. (b) UV-Vis absorption spectra of the different thickness of HAPAN layers (1.3 nm, 5.0 nm, 10 nm, 30 nm) on the quartz glass. (c) AFM height images of bare ITO film, 5.0 nm HAPAN-coated ITO film and 1.3 nm HAPAN-coated ITO film.

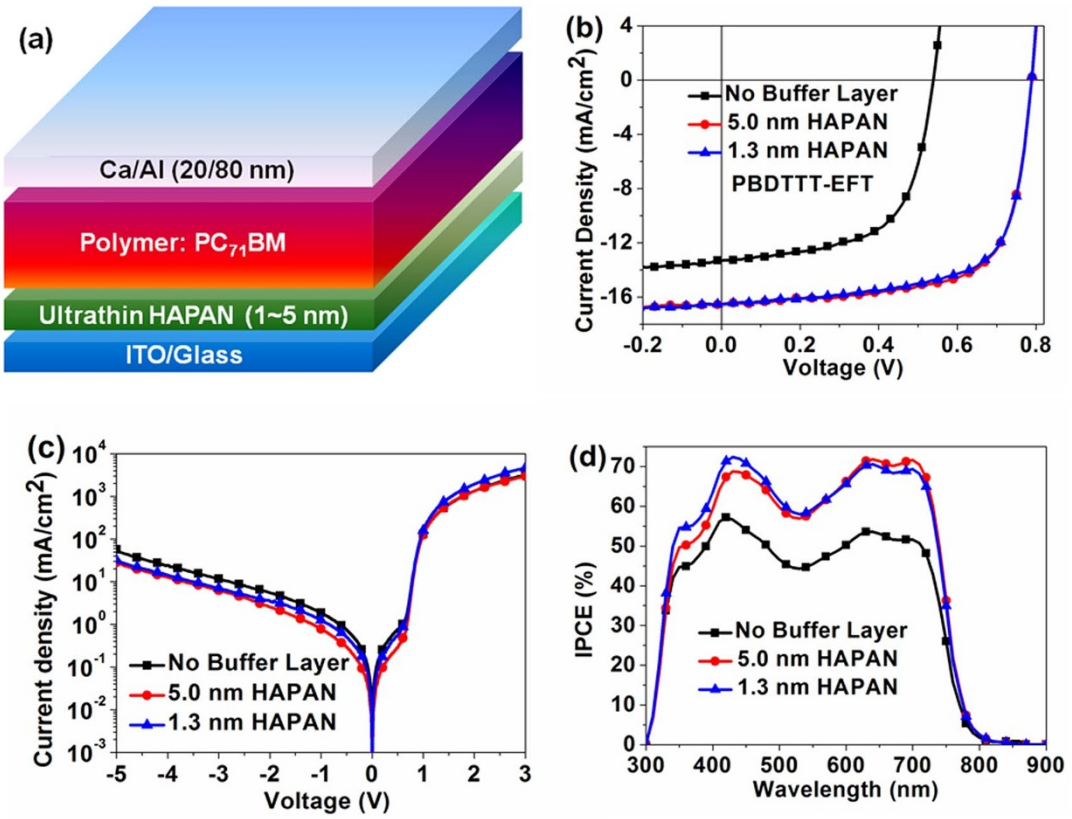

Figure 3 | (a) Device architecture of the conventional PSC utilized in this study; *J-V* characteristics of PBDTTT-EFT based PSC devices employing ultrathin HAPAN with different thickness under (b) 100 mW/cm^2 AM 1.5G illumination and (c) in the dark; (d) The corresponding *EQE* curves of the PBDTTT-EFT based PSC devices employing ultrathin HAPAN with different thickness.

Table 1 | The photovoltaic performance of PBDTTT-EFT/$PC_{71}BM$-based PSC employing HAPAN with different thickness

HAPAN Thickness (nm)	*Voc* (V)	*Jsc* (mA/cm²)	*FF*	PCE_{st} (%)[a]	PCE_{max} (%)[b]	R_s (Ω·cm²)	R_{sh} (KΩ·cm²)
0	0.539	13.32	0.614	4.28 ± 0.28	4.41	8.90	0.51
1.3	0.789	16.54	0.685	8.84 ± 0.10	8.94	7.79	1.03
2.5	0.792	16.32	0.699	8.91 ± 0.09	9.03	7.91	1.94
5.0	0.789	16.51	0.695	9.00 ± 0.12	9.05	7.96	0.89
10	0.790	16.06	0.703	8.81 ± 0.15	8.92	8.18	0.97
20	0.794	15.44	0.709	8.62 ± 0.10	8.69	9.27	1.88
30	0.795	14.32	0.704	7.90 ± 0.08	8.01	9.02	1.54
control device[c]	0.801	16.17	0.678	8.64 ± 0.13	8.78	8.04	1.23

[a]PCE_{st} is the statistical results of 15 devices.
[b]PCE_{max} is the maximum value of the best-performing devices.
[c]Control device is PBDTTT-EFT/$PC_{71}BM$-based PSC device employing PEDOT: PSS (35 nm).

ventional PSC devices. The active layers also exhibited favorable morphology with appropriate nanoscale feature size of ca. 30 nm on the ultrathin HAPAN film. (See AFM and TEM images in Figure S4). It is worth noting that when the thickness of HAPAN is 1.3 nm only, a considerable *PCE* of 8.84 ± 0.10% still can be obtained, and the results reveal that the ITO anode can be effectively modified by coating an ultrathin layer of HAPAN with even 1.3 nm. The series resistance (R_s) and shunt resistance (R_{sh}) were derived from the *J-V* curves. The series resistance (R_s) reduced to 7.96 Ω·cm² and the shunt resistance (R_{sh}) increased to 0.89 kΩ·cm² for the devices with 5.0 nm HAPAN buffer layer. As clearly seen in the dark J-V curves (Figure 3c), a relatively low leakage current and a high rectification ratio was recorded in ultrathin HAPAN-based PSC. In the parallel experiment, the best-performing PSC with PEDOT: PSS (35 nm) as *p*-type EBL showed a slightly lower *PCE* of 8.78% (see Figure S5).

The corresponding incident photon conversion efficiency (IPCE) spectra of the PSCs were characterized and collected in Figure 3d. The J_{sc} values integrated from the IPCE curves were 13.45 mA/cm², 16.45 mA/cm², 16.30 mA/cm² correspond to the no buffer layer, 1.3 nm and 5.0 nm HAPAN device, respectively. Clearly, the J_{sc} values integrated from the IPCE curves agreed well with the J_{sc} of *J-V* tests. Compared with the PSC without *p*-type EBL, the best-performing PSC with 5.0 nm HAPAN film as *p*-type EBL exhibited a higher IPCE ranging from 300 nm to 800 nm, particular in 550 nm–750 nm. The 1.3 nm HAPAN also exhibited better IPCE in the region from 350 nm to 550 nm with a peak value of 72% at 450 nm, indicating efficient photon harvest and charge collection.

In addition, the long-term stability of PSCs based on ultrathin *p*-type EBL was also investigated (see Figure 4 and Figure S6). The PBDTTT-EFT: $PC_{71}BM$-based unencapsulated PSCs in nitrogen glove-box employing 1.3 nm-thick HAPAN was collected and the PSCs employing PEDOT:PSS (35 nm) was also as controls. The *PCE* measured from PEDOT:PSS-based PSC was reduced to 70% of the pristine value within 30 days. In contrast, as observed in Figure 4, the PSC employing the ultrathin HAPAN film as the *p*-type EBL still attained more than 85% of the pristine *PCE* in a long period, which implied the device stability based on ultrathin HAPAN (1.3 nm) is much better than that of PEDOT:PSS (35 nm). The possible reasons might be the morphological changes of the active layer[41], the high pH value as well as minimal usage of ultrathin HAPAN film.

To further investigate the applicability of this ultrathin *p*-type EBL, ultrathin HAPAN was also employed in the other efficient BHJ systems consisting $PC_{71}BM$ and photovoltaic polymers, such as PBDTTT-C-T[9,21], PTB7[20], PBDTBDD[40,42], PBTTDPP-T[43] and PDPP3T[26,44], and their molecular structures were provided in Figure 5a. The identical device fabrication processes were used according to the previous works besides of the *p*-type EBLs. All of the photovoltaic parameters were summarized in Table 2. The similar trends can be observed in PBDTTT-C-T/$PC_{71}BM$, PTB7/$PC_{71}BM$, PBDTBDD/$PC_{71}BM$, PBTTDPP-T/$PC_{71}BM$ and PDPP3T/$PC_{71}BM$-based PSC devices (see Figure 5b–5f). Besides, the ultrathin HAPAN was also utilized in the PSC based on the classical P3HT (see Figure 5g). It can be concluded that the ultrathin HAPAN film is a universal and effective *p*-type EBL for various polymer: PCBM blends.

In summary, PBDTTT-EFT based PSCs with the conventional architecture were fabricated with ultrathin HAPAN film as anode buffer layer, and high *PCEs* of approximately 9% were obtained on only 5.0 nm or 1.3 nm-thick HAPAN film. This study suggests that the application of ultrathin HAPAN film as the anode interfacial layer is also an effective method to improve the device stability. To the best of our knowledge, this is the first report about utilizing ultrathin *p*-type EBLs in highly efficient PSCs. More importantly, this ultrathin layer works well in several efficient photovoltaic polymers including PBDTTT-C-T, PTB7, PBDTBDD, PBTTDPP-T, PDPP3T and P3HT, so it gives a new option for fabricating higher efficiency and long-term stability solar cells as well as ultrathin PSC devices[45]. Further advances in photovoltaic performance would be achieved by optimizing the intrinsic conductivity and pH values of the polyaniline-based *p*-type anode buffer layers.

Methods

Materials. PBDTTT-EFT, PTB7, PDPP3T and $PC_{71}BM$ were commercial available from Solarmer Material Inc. PBDTTT-C-T[21], PBDTBDD[42], PBTTDPP-T[43] were synthesized in our laboratory according to our previous works. The other materials were commercially available and used as received.

Device fabrications. The different concentration HAPAN solution was prepared in distilled water at 60°C for 3 hours in air. The anode buffer layer was spin-coated on pre-cleaned ITO substrates from the HAPAN solution prepared at 4000 rpm for 40 s

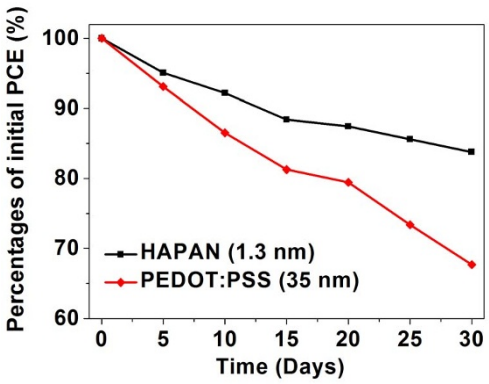

Figure 4 | The long-term stability of the ultrathin HAPAN (1.3 nm) and PEDOT: PSS (35 nm) based-PSC stored in N_2 filled glove box.

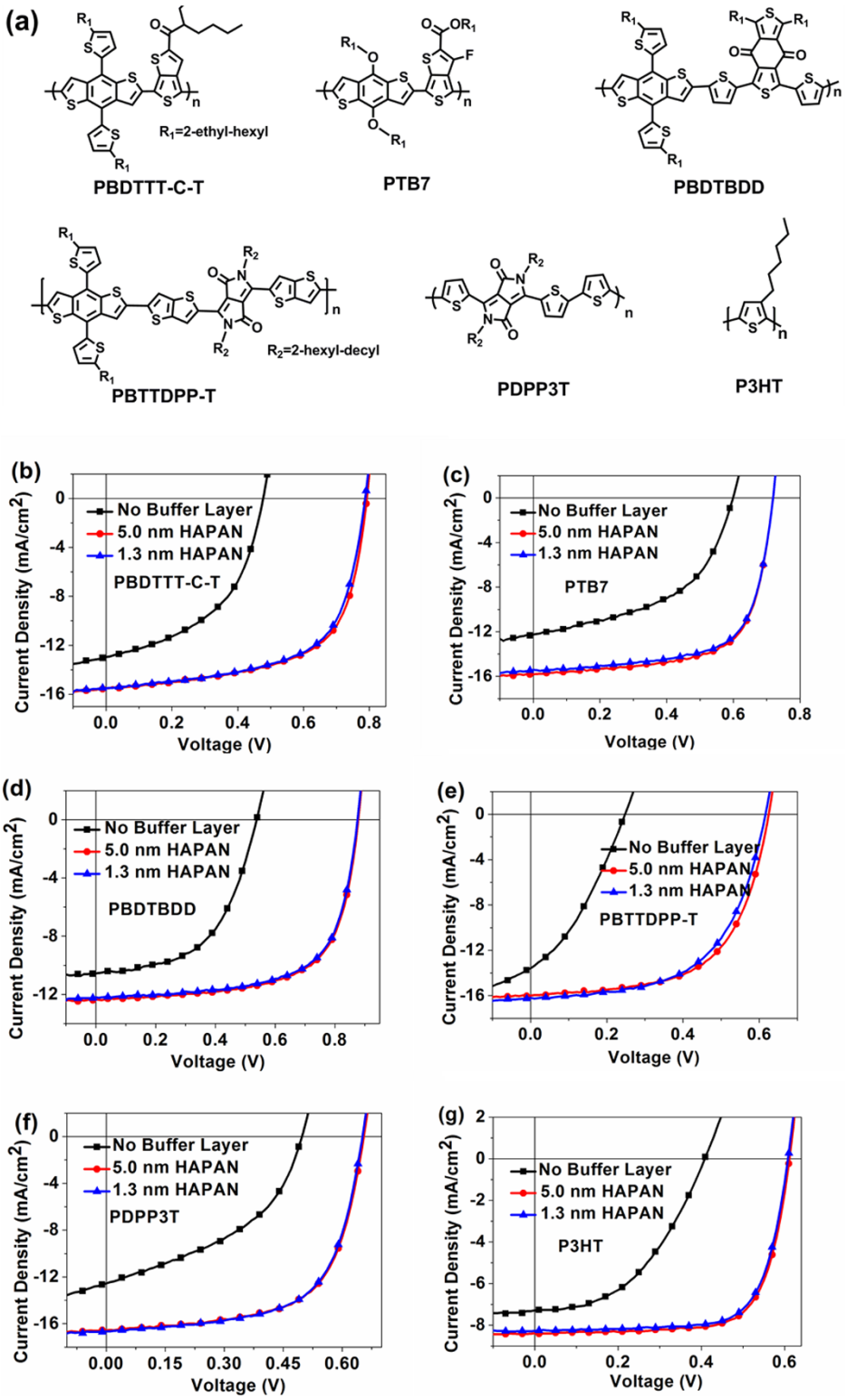

Figure 5 | (a) Molecular structures of other efficient polymers and P3HT; The *J-V* curves of PSC based on (b) PBDTTT-C-T: $PC_{71}BM$, (c) PTB7: $PC_{71}BM$, (d) PBDTBDD: $PC_{71}BM$, (e) PBTTDPP-T: $PC_{71}BM$, (f) PDPP3T: $PC_{71}BM$ and (g) P3HT: $PC_{61}BM$.

and annealed at 150°C for 15 min. The thickness of HAPAN is 1.3 nm, 2.5 nm, 5.0 nm, 10 nm, 20 nm, 30 nm respectively corresponding to a concentration of 1 mg/ml, 2 mg/ml, 4 mg/ml, 10 mg/ml, 20 mg/ml 30 mg/ml. The concentration of PBDTTT-EFT and $PC_{71}BM$ in o-dichlorobenzene (DCB) solution is 10 mg/ml and 15 mg/ml, respectively. These HAPAN films were spin-coated at 4000 rpm for 40 s. The film thickness of HAPAN was verified by several methods such as spectroscopic ellipsometer and the film roughness was characterized using AFM in tapping mode. For morphology modulation, 3% DIO (vol) was added into the blend solution. Blend solutions based on other polymers are prepared according to the previous works and also described in details in Table S2. Prior to evaporating metal cathodes, the blend films were treated with ~60 μL methanol according to our recent report[46]. The device fabrication was completed by thermal evaporation of a 20 nm thick Ca and a 80 nm thick Al layer as cathode under vacuum at a base pressure of 1×10^{-4} Pa.

Table 2 | The photovoltaic properties of PSCs based on several efficient polymer: PCBM blends under AM 1.5G, 100 mW/cm^2 solar illumination

Materials	P-type EBLs	V_{oc} (V)	J_{sc} (mA/cm^2)	*FF*	PCE_{st} (%)	PCE_{max} (%)
PBDTTT-C-T	No Buffer Layer	0.477	12.95	0.481	2.90 ± 0.13	2.97
PBDTTT-C-T	HAPAN (5.0 nm)	0.792	15.50	0.628	7.62 ± 0.07	7.71
PBDTTT-C-T	HAPAN (1.3 nm)	0.787	15.51	0.623	7.51 ± 0.09	7.60
PTB7	No Buffer Layer	0.599	12.24	0.502	3.58 ± 0.12	3.68
PTB7	HAPAN (5.0 nm)	0.719	15.83	0.671	7.55 ± 0.10	7.64
PTB7	HAPAN (1.3 nm)	0.719	15.43	0.676	7.39 ± 0.09	7.50
PBDTBDD	No Buffer Layer	0.538	10.55	0.536	2.93 ± 0.10	3.04
PBDTBDD	HAPAN (5.0 nm)	0.878	12.31	0.666	7.10 ± 0.08	7.20
PBDTBDD	HAPAN (1.3 nm)	0.876	12.19	0.663	6.89 ± 0.11	7.08
PBTTDPP-T	No Buffer Layer	0.248	13.57	0.338	1.02 ± 0.16	1.14
PBTTDPP-T	HAPAN (5.0 nm)	0.625	15.99	0.599	5.91 ± 0.13	5.99
PBTTDPP-T	HAPAN (1.3 nm)	0.616	16.20	0.575	5.62 ± 0.14	5.74
PDPP3T	No Buffer Layer	0.498	12.51	0.475	2.24 ± 0.13	2.96
PDPP3T	HAPAN (5.0 nm)	0.657	16.56	0.656	7.03 ± 0.09	7.13
PDPP3T	HAPAN (1.3 nm)	0.653	16.64	0.648	6.92 ± 0.10	7.04
P3HT	No Buffer Layer	0.408	7.30	0.459	1.32 ± 0.11	1.37
P3HT	HAPAN (5.0 nm)	0.611	8.39	0.722	3.60 ± 0.08	3.70
P3HT	HAPAN (1.3 nm)	0.608	8.27	0.720	3.54 ± 0.12	3.62

1. He, Z., Wu, H. & Cao, Y. Recent Advances in Polymer Solar Cells: Realization of High Device Performance by Incorporating Water/Alcohol-Soluble Conjugated Polymers as Electrode Buffer Layer. *Adv. Mater.* **26**, 1006–1024 (2014).
2. Graetzel, M., Janssen, R. A. J., Mitzi, D. B. & Sargent, E. H. Materials interface engineering for solution-processed photovoltaics. *Nature* **488**, 304–312 (2012).
3. Yip, H. L. & Jen, A. K. Y. Recent advances in solution-processed interfacial materials for efficient and stable polymer solar cells. *Energy Environ. Sci.* **5**, 5994–6011 (2012).
4. Zhou, Y. H. *et al.* A Universal Method to Produce Low-Work Function Electrodes for Organic Electronics. *Science* **336**, 327–332 (2012).
5. He, Z. C. *et al.* Enhanced power-conversion efficiency in polymer solar cells using an inverted device structure. *Nat. Photon.* **6**, 591–595 (2012).
6. Yang, T. B. *et al.* Inverted polymer solar cells with 8.4% efficiency by conjugated polyelectrolyte. *Energy Environ. Sci.* **5**, 8208–8214 (2012).
7. Liu, S. *et al.* High-Efficiency Polymer Solar Cells via the Incorporation of an Amino-Functionalized Conjugated Metallopolymer as a Cathode Interlayer. *J. Am. Chem. Soc.* **135**, 15326–15329 (2013).
8. Li, K. *et al.* Development of Large Band-Gap Conjugated Copolymers for Efficient Regular Single and Tandem Organic Solar Cells. *J. Am. Chem. Soc.* **135**, 13549–13557 (2013).
9. Guo, X. *et al.* Enhanced Photovoltaic Performance by Modulating Surface Composition in Bulk Heterojunction Polymer Solar Cells Based on PBDTTT-C-T/$PC_{71}BM$. *Adv. Mater.* **26**, 4043–4049 (2014).
10. Zhou, Y. H., Fuentes-Hernandez, C., Shim, J. W., Khan, T. M. & Kippelen, B. High performance polymeric charge recombination layer for organic tandem solar cells. *Energy Environ. Sci.* **5**, 9827–9832 (2012).
11. Liao, S.-H., Jhuo, H.-J., Cheng, Y.-S. & Chen, S.-A. Fullerene Derivative-Doped Zinc Oxide Nanofilm as the Cathode of Inverted Polymer Solar Cells with Low-Bandgap Polymer (PTB7-Th) for High Performance. *Adv. Mater.* **25**, 4766–4771 (2013).
12. Chang, C.-Y. *et al.* A Versatile Fluoro-Containing Low-Bandgap Polymer for Efficient Semitransparent and Tandem Polymer Solar Cells. *Adv. Funct. Mater.* **23**, 5084–5090 (2013).
13. Sun, Y. *et al.* Chemically Doped and Cross-linked Hole-Transporting Materials as an Efficient Anode Buffer Layer for Polymer Solar Cells. *Chem. Mater.* **23**, 5006–5015 (2011).
14. Chang, Y. M. *et al.* Electrostatic Self-Assembly Conjugated Polyelectrolyte-Surfactant Complex as an Interlayer for High Performance Polymer Solar Cells. *Adv. Funct. Mater.* **22**, 3284–3289 (2012).
15. Gu, C. *et al.* Electrochemical Route to Fabricate Film-Like Conjugated Microporous Polymers and Application for Organic Electronics. *Adv. Mater.* **25**, 3443–3448 (2013).
16. Zhou, H. *et al.* Conductive Conjugated Polyelectrolyte as Hole-Transporting Layer for Organic Bulk Heterojunction Solar Cells. *Adv. Mater.* **26**, 780–785 (2014).
17. You, J. *et al.* A polymer tandem solar cell with 10.6% power conversion efficiency. *Nat. Commun.* **4**, 1446 (2013).
18. Li, Y. F. Molecular Design of Photovoltaic Materials for Polymer Solar Cells: Toward Suitable Electronic Energy Levels and Broad Absorption. *Acc. Chem. Res.* **45**, 723–733 (2012).
19. Chen, H. Y. *et al.* Polymer solar cells with enhanced open-circuit voltage and efficiency. *Nat. Photon.* **3**, 649–653 (2009).
20. Liang, Y. Y. *et al.* For the Bright Future-Bulk Heterojunction Polymer Solar Cells with Power Conversion Efficiency of 7.4%. *Adv. Mater.* **22**, E135–E138 (2010).
21. Huo, L. J. *et al.* Replacing Alkoxy Groups with Alkylthienyl Groups: A Feasible Approach To Improve the Properties of Photovoltaic Polymers. *Angew. Chem. Int. Ed.* **50**, 9697–9702 (2011).
22. Ye, L., Zhang, S., Zhao, W., Yao, H. & Hou, J. Highly Efficient 2D-Conjugated Benzodithiophene-Based Photovoltaic Polymer with Linear Alkylthio Side Chain. *Chem. Mater.* **26**, 3603–3605 (2014).
23. Wang, M. *et al.* Donor Acceptor Conjugated Polymer Based on Naphtho[1,2-c:5,6-c]bis[1,2,5]thiadiazole for High-Performance Polymer Solar Cells. *J. Am. Chem. Soc.* **133**, 9638–9641 (2011).
24. Dou, L. T. *et al.* A Selenium-Substituted Low-Bandgap Polymer with Versatile Photovoltaic Applications. *Adv. Mater.* **25**, 825–831 (2013).
25. Cabanetos, C. *et al.* Linear Side Chains in Benzo[1,2-b:4,5-b′]dithiophene-Thieno[3,4-c]pyrrole-4,6-dione Polymers Direct Self-Assembly and Solar Cell Performance. *J. Am. Chem. Soc.* **135**, 4656–4659 (2013).
26. Li, W., Furlan, A., Hendriks, K. H., Wienk, M. M. & Janssen, R. A. J. Efficient Tandem and Triple-Junction Polymer Solar Cells. *J. Am. Chem. Soc.* **135**, 5529–5532 (2013).
27. Guo, X. *et al.* Polymer solar cells with enhanced fill factors. *Nat. Photon.* **7**, 825–833 (2013).
28. Gustafsson, G. *et al.* Flexible Light-Emitting-Diodes Made from Soluble Conducting Polymers. *Nature* **357**, 477–479 (1992).
29. Cao, Y., Smith, P. & Heeger, A. J. Counterion Induced Processibility of Conducting Polyaniline and of Conducting Polyblends of Polyaniline in Bulk Polymers. *Synth. Met.* **48**, 91–97 (1992).
30. Meng, Y. N., Wang, K., Zhang, Y. J. & Wei, Z. X. Hierarchical Porous Graphene/Polyaniline Composite Film with Superior Rate Performance for Flexible Supercapacitors. *Adv. Mater.* **25**, 6985–6990 (2013).
31. Zou, W. *et al.* Biomimetic Superhelical Conducting Microfibers with Homochirality for Enantioselective Sensing. *J. Am. Chem. Soc.* **136**, 578–581 (2013).
32. Chen, S. A. & Hwang, G. W. Synthesis of Water-Soluble Self-Acid-Doped Polyaniline. *J. Am. Chem. Soc.* **116**, 7939–7940 (1994).
33. Fan, B. *et al.* Improved performance of cyanine solar cells with polyaniline anodes. *J. Mater. Chem.* **20**, 2952–2955 (2010).
34. Jung, J. W., Lee, J. U. & Jo, W. H. High-Efficiency Polymer Solar Cells with Water-Soluble and Self-Doped Conducting Polyaniline Graft Copolymer as Hole Transport Layer. *J. Phys. Chem. C* **114**, 633–637 (2010).
35. Ke, W. J. *et al.* Solution processable self-doped polyaniline as hole transport layer for inverted polymer solar cells. *J. Mater. Chem.* **21**, 13483–13489 (2011).
36. Abdulrazzaq, O. *et al.* Optimization of the Protonation Level of Polyaniline-Based Hole-Transport Layers in Bulk-Heterojunction Organic Solar Cells. *Energy Technology* **1**, 463–470 (2013).
37. Ito, S. *et al.* Simple synthesis of water-soluble conducting polyaniline. *Synth. Met.* **96**, 161–163 (1998).
38. Tan, Z. *et al.* Solution-Processed Rhenium Oxide: A Versatile Anode Buffer Layer for High Performance Polymer Solar Cells with Enhanced Light Harvest. *Adv. Energy Mater.* **4**, DOI: 10.1002/aenm.201300884 (2014).
39. Liu, P. *et al.* Effect of Fluorine Content in Thienothiophene-Benzodithiophene Copolymers on the Morphology and Performance of Polymer Solar Cells. *Chem. Mater.* **26**, 3009–3017 (2014).
40. Tan, Z. *et al.* High performance polymer solar cells with as-prepared zirconium acetylacetonate film as cathode buffer layer. *Sci. Rep.* **4**, 4691 (2014).
41. Li, W. *et al.* The Effect of additive on performance and shelf-stability of HSX-1/PCBM photovoltaic devices. *Org. Electron.* **12**, 1544–1551 (2011).

42. Qian, D. *et al*. Design, Application, and Morphology Study of a New Photovoltaic Polymer with Strong Aggregation in Solution State. *Macromolecules* **45**, 9611–9617 (2012).
43. Zhang, S. *et al*. Enhanced Photovoltaic Performance of Diketopyrrolopyrrole (DPP)-Based Polymers with Extended π Conjugation. *J. Phys. Chem. C* **117**, 9550–9557 (2013).
44. Ye, L. *et al*. From Binary to Ternary Solvent: Morphology Fine-tuning of D/A Blends in PDPP3T-based Polymer Solar Cells. *Adv. Mater.* **24**, 6335–6341 (2012).
45. Kaltenbrunner, M. *et al*. Ultrathin and lightweight organic solar cells with high flexibility. *Nat. Commun.* **3**, 770 (2012).
46. Ye, L. *et al*. Remove the Residual Additives toward Enhanced Efficiency with Higher Reproducibility in Polymer Solar Cells. *J. Phys. Chem. C* **117**, 14920–14928 (2013).

Acknowledgments

This work was supported by National Basic Research Program 973 (2014CB643500), International S&T Cooperation Program of China (2011DFG63460), the Science and Technology Commission of Beijing (Z131100006013002), the Chinese Academy of Sciences (Nos. XDB12030200, KJZD-EW-J01), NSFC (21274134) and New Century Excellent Talents in University (NCET-11-0473).

Author contributions

J.H.H., L.Y. and W.C.Z. conceived the idea. W.C.Z. and L.Y. carried out device fabrication and characterization of the devices, data collection and analysis. B.F. synthesized the polyaniline interlayer and S.Q.Z. contributed to the photovoltaic polymers. W.C.Z., L.Y., M.L.S. and J.H.H. prepared the first draft. All authors discussed the results and provided comments on the manuscript. J.H.H. directed the research.

Additional information

Supplementary information accompanies this paper at http://www.nature.com/scientificreports

Competing financial interests: The authors declare no competing financial interests.

How to cite this article: Zhao, W. *et al*. Ultrathin Polyaniline-based Buffer Layer for Highly Efficient Polymer Solar Cells with Wide Applicability. *Sci. Rep.* **4**, 6570; DOI:10.1038/srep06570 (2014).